Strong temporal and spatial variation of dissolved Cu isotope composition in acid mine drainage under contrasted hydrological conditions

Masbou[1,2] J., Viers[1]* J., Grande[3] J-A., Freydier[4] R., Zouiten[1] C., Seyler[4] P., Pokrovsky[1,5] O., Behra[6] P., Dubreuil[6] B., de la Torre[3] M-L.

1 : Géosciences Environnement Toulouse (GET), Université de Toulouse, CNRS, IRD 14 avenue Edouard Belin, 31400 Toulouse, France
2 : Laboratoire d'Hydrologie et de Géochimie de Strasbourg (LHyGeS), Université de Strasbourg/ENGEES, CNRS, 1 rue Blessig, 67084, Strasbourg Cedex, France
3 : Centro de Investigación para la Ingeniería en Minería Sostenible, Escuela Técnica Superior de Ingeniería, Universidad de Huelva, Ctra. Palos de la Frontera, s/n, 21819 Palos de la Frontera, Huelva, Spain
4 : Laboratoire HydroSciences UMR 5569, CNRS, IRD, Université de Montpellier, 163 Rue Auguste Broussonnet, CC 57, 34090, Montpellier, France
5 : BIO-GEO-CLIM Laboratory, Tomsk State University, 36 Lenina Prs, Tomsk, Russia
6 : Laboratoire de Chimie Agro-industrielle, LCA, Université de Toulouse, INRA, Toulouse, France

* Corresponding author: Jerôme Viers, Ph.D.

Abstract

Copper export and mobility in acid mine drainage are difficult to understand with conventional approaches. Within this context, Cu isotopes could be a powerful tool and here we have examined the relative abundance of dissolved (< 0.22 µm) Cu isotopes (δ^{65}Cu) in the Meca River which is an outlet of the Tharsis mine, one of the largest abandoned mines of the Iberian Pyrite Belt, Spain. We followed the chemical and isotopic composition of the upstream and downstream points of the catchment during a 24-h diel cycle. Additional δ^{65}Cu values were obtained from the tributary stream, suspended matter (> 0.22 µm) and bed sediments samples. Our goals were to *1)* assess Cu sources variability at the upstream point under contrasted hydrological conditions and *2)* investigate the conservative vs. non conservative Cu behavior along a stream. Average δ^{65}Cu values varied from -0.47 to -0.08 ‰ (n= 9) upstream and from -0.63 to -0.31‰ downstream (n = 7) demonstrating that Cu isotopes are heterogeneous over the diel cycle and along the Meca River. During dry conditions, at the upstream point of the Meca River the Cu isotopic composition was heavier which is in agreement with the preferential release of heavy isotopes during the oxidative dissolution of

primary sulfides. The more negative values obtained during high water flow are explained by the contribution of soil and waste deposit weathering. Finally, a comparison of upstream vs. downstream Cu isotope composition is consistent with a conservative behavior of Cu, and isotope mass balance calculations estimate that 87 % of dissolved Cu detected downstream originate from the Tharsis mine outlet. These interpretations were supported by thermodynamic modelling and sediment characterisation data (X-ray diffraction, Raman Spectroscopy). Overall, based on contrasted hydrological conditions (dry vs flooded), and taking the advantage of isotope insensitivity to dilution, the present work demonstrates the efficiency of using the Cu isotopes approach for tracing sources and processes in the AMD regions.

Keywords: copper; isotopes, Acid Mine Drainage (AMD); river; flood

1. Introduction

The Iberian Pyrite Belt (South-west Spain), which is among the largest metallogenic provinces in the world, presents serious problems of Acid Mine Drainage (AMD) (Almodovar et al., 1997; Leblanc et al., 2000 ; Grande et al., 2010, 2013; Olias et al., 2019) due to the intense mining activity that occurred during different periods ofhistory including the present time. In particular, during the most active period, from the mid-XIXth to the XXth centuries, large amounts of abandoned waste have been left over the whole region (Pérez Ostalé, 2014). Induced AMD phenomenon leads to surface waters with low pH, and a high metal and sulphate load that strongly affect both inland and marine ecosystems since the two largest AMD affected watersheds of the region, the Odiel and Tinto Rivers, deliver their waters to the estuary of Huelva (Achterberg et al., 2003; Sainz et al., 2004; Nieto et al., 2007; Grande et al., 2018). Due to scarcity of water in this region of the South-West of Europe, the AMD can strongly impact the aquatic ecosystems and surface and groundwater quality (see

65 www.fao.org). Despite the numerous studies dealing with the AMD processes origins and
66 consequences on waters, soils and biota (e.g., Elbaz-Poulichet et al., 2001) the metal
67 distribution, reactivity and transport mechanisms in the rivers still remain poorly known.
68 In addition to dissolved and particulate metals concentrations monitoring in surface waters,
69 the stable isotopes of metals (Cu, Fe, Zn…) are now routinely used to trace the source of
70 metals in the environment and to reveal the biotic and abiotic mechanisms controlling
71 elements transfer within a watershed (see Teng et al. (2017) for a review). As most of the
72 mines in the Iberian Pyrite Belt were mined for copper (Saez et al., 1999), we looked at the
73 potential contribution of copper isotopes to better understand this metal behaviour in such
74 areas. A number of works addressed Cu isotopes in the AMD context (Mathur et al., 2005;
75 Balistrieri et al., 2008; Borrok et al., 2008; Fernandez and Borrok, 2009; Kimball et al., 2009;
76 Mathur et al., 2009; Pérez Rodríguez et al., 2013; Mathur et al., 2014; Song et al., 2016;
77 Dótor-Almazán et al., 2017; Viers et al., 2018; Roebbert et al., 2018). Carried out during
78 steady hydrological conditions, these studies showed that sulfide mineral dissolution in
79 oxygenic conditions essentially controls the Cu isotopes distribution in surface and ground
80 waters. Extensive natural observations and experimental works evidenced strong enrichment
81 in heavy Cu isotopes of aqueous solution interacting with primary sulfide minerals. Moreover,
82 in contrast to relatively narrow range of isotopic signature (δ^{65}Cu) in these primary minerals,
83 the secondary mineral products exhibit a δ^{65}Cu variability as high as from -17 to + 10 ‰, see
84 (Mathur et al., 2009). The speciation of Cu in sulfide mine environments is extremely
85 complex because Cu is present in numerous secondary minerals whose proportions strongly
86 depend on the hydrological regime (wetting and drying) (Valente et al., 2013). Moreover, the
87 formation of these minerals in mine-impacted surface waters is controlled by key parameters
88 such as pH, temperature, redox conditions, saturation state and biological activity (Sanchez-
89 Espana et al., 2005, 2011; Sarmiento et al., 2009a,b). High sensitivity to fractionation of

copper isotopes in supergene environments makes copper isotopes a good potential tracer for metal transfer within the continuum mine – river – lake encountered in the Iberian Pyrite Belt.

To better understand the environmental factors controlling Cu concentration and isotopes fractionation in AMD aquatic settings, our initial objective was to study the evolution of chemical and isotopic fractionation during a diel cycle (24h) in an AMD impacted river. Indeed, several parameters and processes that are often interrelated (T°, dissolved O_2, water discharge, pH…) may influence the concentration of the chemical species during a diel cycle in the water (Nimick et al., 2011). To address this issue within the AMD context, we used a representative scenario of strongly contaminated Meca River (Huelva, SW Spain) of the Iberian Pyrite Belt. This river drains the abandoned copper mine of Tharsis - one of the largest in the area - and delivers its waters to the Sancho Lake. Taking the advantage of an extremely strong rainy event that occurred during the sampling period, we primarily focused on studying the response of a mining system to variable hydrological stage. Further, in order to quantify the spatial variability of Cu isotope composition in the AMD-affected Meca River, we performed measurements in two points, one at the outlet of the mining district and one 20 km downstream, three hours each during 24 hours. We expected that by examining the variation of Cu isotopic composition in time and space, we can better understand the transfer and origin of Cu and other metals within the mining area and reveal the mechanisms of Cu isotopes fractionation in these environmentally important riverine systems.

2. Site description

2.1. Geology of the Iberian Pyrite Belt

The study area belongs to the Iberian Pyrite Belt (IPB), located in the south-west of the Iberian Peninsula.This IPB is approximately 240 km long and 50 km wide and is one of the

largest stocks of massive sulfides of volcanogenic origin in the world. It includes more than 90 mines (Saez et al., 1999). Pyrite (FeS_2) is the main ore mineral but one finds a procession of other metallic sulfides such as sphalerite (ZnS), galena (PbS), chalcopyrite ($CuFeS_2$), arsenopyrite (FeAsS) and there is a large variety of other metal sulfides containing minor quantities of Cd, Sn, Ag, Au, Co, Hg. Today, the majority of these mines are abandoned even though some remain in operation. Details about the geology of this area can be found in Tornos et al. (2008) and Conde et al. (2009).

2.2. Hydroclimatic conditions

The study area, located in the Huelva province, has a Mediterranean climate, which can be classified as semi-arid. Annual precipitation is about 630 mm/year, being mostly concentrated in the wet season from October to May, and the average annual temperature is 17.1 ºC (http://www.aemet.es).

Our study took place in the watershed of the Meca River, a tributary of the Odiel River. The Odiel River joins the Tinto River at the city of Huelva. The average water discharge of the Odiel River is around 10 $m^3.s^{-1}$ at Gibraleon, a town close to the river mouth (see ConfederacionHidrografica del Guadiana; https://www.chguadiana.es). The Odiel watershed with a surface of 2300 km^2 and a length of 140 km accounts for about 80% of the continental water reaching the estuary of Huelva (Santisteban, 2015). The whole river network is impacted by acid mine drainage (Grande et al., 2018). This is especially correct for the Meca River due to the presence of the Tharsis mine, in the upstream part of its catchment. Although it is now abandoned, Tharsis is one of the largest mining districts with almost 100 Mt of estimated resources (Conde et al., 2009). Further details of the Tharsis mine can be found in Perez Ostale (2014) and Valente et al. (2013).

The weather was particularly rainy during the field sampling (11 to 12-May-2016). It rained 58 mm the preceding three days (8 to 10-May-2016) to our sampling (Alosno station) and 24 mm on the 11-May-2016. Unfortunately, we do not have the whole dataset for rain water because the weather station was destroyed during this storm event; As the Meca River water discharge is not monitored continuously, we performed a measurement of the water discharge using the "bucket method" when it was possible. Using previous work done by Galvan et al. (2009) within the Meca River catchment, sulphate concentrations could be used in the first order to account for the relative variation in water discharge. Indeed, these authors proposed the following relation between sulphate concentration (SO_4) and water discharge (Q) : ($[SO_4] = 362.1*Q^{-0.30}$).No relation was proposed by these authors between Cu concentration and Q due to the lack of reproducibility.

3. Materials and methods

3.1. Sampling protocol

Sampling strategy aimed to study the geochemical processes along the Meca River during a complete diel cycle (24 h). Geographical gradient was investigated by collecting water samples simultaneously by two different teams in two sampling sites (Fig. 1): *i)* the Tharsis Mine outlet located upstream of the watershed called 'upstream' and *ii)* a point located 20 km downstream (called 'downstream'). Sampling was achieved in a similar timeframe of 24h for the two sites, between 11-May-2016 4:00 p.m. and 12-May-2016 5:00 p.m. with a time step of 3 hours. In addition, one sample of the main Meca tributary (between the two points) was also collected (Tributary stream, Fig. 1). In addition to water samples, a bedload sediment sample from the Meca River was collected at the upstream point.

At each sampling point, the values of pH, dissolved O_2, temperature, and specific conductivity were measured *in-situ* using a portable multi-parameter instrument (WTW®, 340i). Protocols for the measurement of these parameters and the sampling method are reported in Viers et al. (2018). Among the collected samples, the 0.22 µm membrane of four selected samples were conserved to recover suspended sediments and perform chemical analyses. In addition to 0.22 µm filtration, an ultrafiltration at 1,000 Da were carried out on four selected samples collected upstream (11-May-2016 4:00 p.m., 11-May-2016 10:00 p.m., 12-May-2016 4:00 a.m., 12-May-2016 10:00 a.m.) using a 50 mL Amicon® ultrafiltration cell. Details of ultrafiltration procedure, analyses of possible artifacts and yields are given elsewhere (Viers et al., 1997; Dupré et al., 1999; Vasyukova et al., 2010).

3.2. Mineralogical characterization

Two suspended sediments collected at the upstream point (ME-A 11-May-2016 10 p.m. and ME-A 12-May-2016 4 p.m. samples) were characterised by SEM-EDX (form, chemical composition) at the Centre de MicroCaractérisationRaimondCastaing (Toulouse) and by X-Ray Diffraction at the GET laboratory (Toulouse). All the details about the methods are reported in Blondet et al. (2019) and Blotevogel et al. (2018).

The Raman spectra of the ME-A 11-May-2016 10 p.m. sample was obtained at room temperature by the confocal microscope Raman spectrometer (Horiba Scientific Labram HR evolution spectrometer) equipped with charge coupled device (CCD) as detector at the LCA laboratory of the Ensiacet (INPT). We used the 532 nm laser as excitation source and a dry objective MPLN x100 (NA: 0.90 µm). Measurement conditions were: laser power of 2.5 mW during 1 second and 2 accumulations; pinhole: 100 µm; spectral range: 100 to 2400 cm^{-1} scanned with a high-resolution grating with 1800 gr/mm; Raman spectra: recorded directly

from powder. Raman spectral libraries from Bio-Rad and KnowltAll® ID ExpertTM spectroscopy software were used for the identification.

3.3. Elemental content determination (major and Trace Elements (TE))

Major and trace element concentrations were measured using ICP-MS (iCAP Q, Thermo Scientific- Kinetic Energy Discrimination mode using He) at the AETE-ISO platform (OSU OREME/Université de Montpellier). Concentrations were determined with external calibration using (Be, Sc, Ge, Rh, Ir) as internal standards to correct potential sensitivity drifts. The quality of the analysis was checked by analyzing international certified reference waters (CNRC SLRS-6). The accuracy was better than 5% relative to the certified values and the analytical error (relative standard deviation) was better than 5% for concentrations ten times higher than the detection limits. Anions concentrations were determined by ionic chromatography at the GET laboratory.

In addition to total measurements, Fe speciation (Fe^{2+} and Fe^{3+}) was determined by spectrophotometry and on-site using ferrozine method (Viollier et al., 2000). These measurements were performed on the dissolved fraction (<0.22 µm) immediately after sampling for the upstream samples.

Before analysis, sediments were digested at the GET laboratory. For each sample, 100 mg of sediment were precisely weighed in Teflon vessels. 1 mL of H_2O_2 and 0.5 mL of bidistilled HNO_3 were added to the samples and left at room temperature for 24 hours. Then, 1 mL of HNO_3 is added and the solutions were warmed at 80°C for 24 h. The solution is then evaporated on a plate at 80°C. 1.2 ml of HF and 1.2 ml of bidistilled HNO_3 are then added for a new warming step at 80°C. After evaporation, 20 drops of bidistilled HCL and 10 drops of bidistilled HNO_3 are added. The acid solution was warmed at 115°C for 24 h and finally

209 evaporated at 80°C. After complete evaporation, the remaining solid residue for each sample
210 was dissolved in 10 mL of a 10% HNO_3 solution. Acid blanks and certified reference material
211 samples (LKSD-03, lake sediment samples) were also used to ensure the quality of the
212 measures and their traceability.
213
214 *3.4. Cu isotopes determination*

215 Water sample aliquots containing approximately 1000 ng of Cu were purified using anion
216 exchange chromatography on AG-MP1 resin (BIORAD) following an adapted protocol from
217 Borrok et al. (2008). The protocol was repeated twice in order to ensure a complete separation
218 of Cu from the matrix. The total procedure blank was negligible in comparison with the
219 amount of Cu in the samples (<1%). Column yields and remaining elements such as (Na, Mg,
220 Ca, Ti, Cr) that can interfere with Cu and Zn isotopes (Petit et al., 2008) were checked for
221 each samples using Q-ICP-MS iCAP Q (Thermo Scientific). The yield was 100 ± 5% and no
222 interfering elements were found in the solutions. Cu isotopic analyses were performed on a
223 multiple-collector inductively coupled plasma mass spectrometer (MC-ICP-MS) Neptune
224 Plus (Thermo Scientific®), using SIS (Stable introduction System) nebulization chamber and
225 PFA self-aspiration nebulizer (50 $\mu l.min^{-1}$, Elemental Scientific®) at Plateforme AETE-ISO
226 (OSU OREME-Université de Montpellier, France). Each sample was analyzed three times
227 and was bracketed with the SRM NIST 976 copper solution. Cu isotopes (^{63}Cu, ^{65}Cu), Zn
228 isotopes (^{64}Zn, ^{66}Zn, ^{67}Zn, ^{68}Zn), and Ni isotope (^{62}Ni) were monitored simultaneously.
229 Measurements of ^{62}Ni signal allowed correcting the possible isobaric interference of ^{64}Ni on
230 ^{64}Zn. A Zn solution JMC 3e0749-L from Lyon was added to the samples in order to correct
231 instrumental mass bias using the $^{66}Zn/^{64}Zn$ ratio (exponential law) and the method of sample-
232 standard bracketing was used to determine the $\delta^{65}Cu$ (Marechal et al., 1999). The 2σ variation
233 obtained on the 3 independent $\delta^{65}Cu$ measurements was 0.01-0.06 ‰.

δ^{65}Cu (in units of ‰) is the Cu isotopic deviation relative to a standard, the SRM NIST-976:

$$\delta\ {}^{65}Cu = \left(\left(\frac{\left(\frac{^{65}Cu}{^{63}Cu}\right)_{sample}}{\left(\frac{^{65}Cu}{^{63}Cu}\right)_{NIST976}} \right) - 1 \right) \times 1000$$

2.3. Thermodynamic calculations

Thermodynamic analysis including calculations of the speciation and the saturation indexes have been performed for the Meca River (upstream and downstream points) with respect to the common minerals of mining environments and specifically those described for the Tharsis mine by previous studies (Sanchez-Espana et al., 2005; Valente et al., 2013). Following these studies, we considered that goethite, ferrihydrite, jarosite, gibbsite, schwertmannite, (hydro)basaluminite, and gypsum may precipitate from aqueous solution. Modelling calculations were done using Visual MINTEQ ver. 3.0. In the case of the minerals schwertmannite and hydrobasaluminitethe solubility product constants (log K_{sp}) were taken from Sanchez-Espana et al. (2011) and the calculations were done manually using the element activities given by Visual Minteq 3.0. It is visible that their value for schwertmannite (log K_{sp} = 18.8 ± 3.5; pH range = 2.6 – 5.2) is very similar to that proposed by Bigham et al. (1996) (log K_{sp} = 18.0 ± 2.5; pH range = 2.8 – 3.2). The results of speciation and saturation indexes are reported in the supplementary information (Table S1 A and B).

3. Results

3.1. Variation of the water conductivity and pH in the Meca River

In the upstream point, conductivity varies from 2.8 to 11.4 mS/cm and pH varies between 2.43 and 2.82 (Table 1). At the downstream point, conductivity is much lower (from 0.31 to 0.54 mS/cm) and pH is higher with values ranging between 3.61 and 5.68. The Meca tributary exhibits intermediate values with a pH of 3.85 and a conductivity of 0.51 mS/cm.

Element concentrations in the river water are reported in Table 1. At the upstream point, the anionic load is dominated by SO_4^{2-} (> 99%) and the cationic load is dominated by Fe (> 50%), Mg^{2+} (> 20%), Al^{3+} (> 15%), Zn^{2+} and Ca^{2+} (> 4%) and Cu^{2+} (~1%). At the downstream point, the anionic load is dominated by SO_4^{2-} (> 60%) and Cl^- (> 30%) while the cationic load is dominated by Mg^{2+} (> 35%), Na^+ (> 30%), Ca^{2+} (> 20%), and Fe (> 6%). Copper accounts for less than 0.5% of the cationic load at the downstream point. In the Meca tributary, the anionic load is dominated by SO_4^{2-} (70%), followed by Cl^- and NO_3^- (15%). The cationic load is dominated by Mg^{2+} (40%), Ca^{2+} (30%) and Na^+ (20%). Elemental concentrations are generally much lower in the downstream sampling point (e.g., 80 times for Cu) because of dilution process. However, we note that Cl, NO_3 and K concentrations are higher in the downstream sampling point while Na concentration is rather similar in the two sampling points.

3.2. Copper concentration and isotope composition of Meca River

Upstream, dissolved Cu concentrations range from ~17 mg/L to ~120 mg/L and insignificant differences have been detected between concentrations in the < 0.22 µm fraction and in the < 1,000 Da fraction (see Table 1), revealing the absence of Cu in the colloidal phase (1 kDa - 0.22 µm). Copper concentrations obtained during this campaign are in good agreement with those measured previously in the Odiel watershed and its sub-watersheds

278 (e.g., Sanchez Espana et al., 2005; Sarmiento et al., 2009a,b; Grande et al., 2010; Moreno
279 Gonzalez et al., 2020). Dissolved Cu concentrations decrease to 0.29 - 1.65 mg/L in the
280 downstream point. In both sampling points, dissolved Cu is highly correlated with SO_4
281 (R^2=0.99 between Cu and SO_4), Fe concentrations (Fig. 2 and 3) and other elements. To
282 illustrate the link between these elements, we reported the relationship obtained between Cu
283 and Ni concentrations for both upstream and downstream points (Figure SI-1). In order to
284 explore multiple correlations between parameters (time, concentrations….), a Partial Least
285 Square Analysis method was necessary since we have more variables than individuals (Wold,
286 1985; Abdi, 2010) (see Fig. SI-2). The inertia graph reveals that only one single factor is
287 interpretable (Fig. SI-2A). The two sites are clearly distinguished by their chemical
288 composition and by the evolution of concentrations through time (see Fig. SI-2C). In the
289 upstream point Cu and other element concentrations vary simultaneously as a function of time
290 (and water discharge variation) while concentrations are much more stable at the downstream
291 point.

292 Copper isotope compositions range from -0.47 to -0.08 ‰ (n = 9) and -0.63 to -0.31(n = 7)
293 ‰ at upstream and downstream point, respectively (Table 1). These values are coherent but
294 more variable than those previously obtained in a similar context (-0.75 ± 0.13 ‰ in the Odiel
295 River,Borrok et al., 2008). Cu isotope composition of the Meca River suspended matter
296 collected on 12-May-2016 at 4:00 p.m. ($\delta^{65}Cu_{suspended\text{-}matter}$= -0.41 ± 0.03 ‰) is the same as
297 that of filtered water ($\delta^{65}Cu_{Dissolved}$ = -0.42 ± 0.01 ‰, Table 2). On the contrary, the top layers
298 of bed sediments of the Meca River revealed more negative $\delta^{65}Cu_{sediment}$ of -1.92 ± 0.04 ‰.

299 Copper dissolved concentration and δ^{65}Cu values showed significant variation over a 24-h
300 period (Fig. 4). The upstream δ^{65}Cu values fluctuate between -0.47 ± 0.01‰ (2σ) and -0.08 ±
301 0.02 ‰ (2σ). During high rainfall periods (high discharge regime), lower Cu concentrations
302 (≈ 17 mg/L) and δ^{65}Cu values (≈ -0.4 ‰) associated with higher pH (> 2.80) are observed.

303 During low water discharge period, we observe higher Cu concentrations (up to 120 mg/L),
304 lower pH (pH < 2.5) and higher δ^{65}Cu values (close to 0 ‰). In the downstream point, where
305 Cu concentrations are much lower, from 0.29 to 1.65 mg/L, the δ^{65}Cu is between -0.31 and -
306 0.63‰: Thus we observe similar tendency as in the upstream point with concomitant lower
307 δ^{65}Cu and Cu content.
308
309 *3.3. The suspended sediment of the Meca River: mineralogical characterization and chemical*
310 *analysis*

311 Two suspended matter samples from the Meca River upstream point (ME-A 11-May-2016
312 10:00 p.m.; ME-A 12-May-2016 4:00 p.m.,) were studied using SEM-EDS and X-ray
313 diffraction while Raman spectroscopy has been performed on the ME-A 11-May-2016 10:00
314 p.m. sample.

315 The SEM observations of both samples revealed homogeneous composition of suspended
316 material. We note the predominance of a muscovite type mineral (see Fig. SI-3 supplementary
317 information) in both samples and the presence of quartz, Fe oxides, rutile (TiO_2) and grains
318 containing S + Fe + As + Pb or S + Fe + Pb or S + Fe associations. Based on results of the X-
319 ray diffraction (see Fig. SI-4), the mineral containing S + Fe + Pb + As appears to be a
320 beudantite type mineral, the mineral containing S + Fe is a copiapite type mineral and the
321 mineral containing S + Fe + Pb is a (plumbo)jarosite type mineral. Pyrite, Ti oxides, and Fe
322 oxides grains have been also observed in the ME-A 11-May-2016 10:00 p.m. sample. The
323 EDS system of the SEM did not allow detecting Cu in the investigated minerals. Raman
324 spectroscopy revealed the presence of Fe oxydes, Tioxydes, jarosite, plumbojarosite and
325 wavellite (hydrated aluminous phosphate) confirming the X-ray diffraction data (Fig. SI-5).

326 Collected sediments were mainly composed of Fe, Al, K and Pb (between 1 and 10%)
327 and contained Mg, Ti, As, Na, Zn, Sb and Cu as minor elements with concentrations between

0.1 and 1%. Due to our analytical protocol, Si and S were not analysed in the solids. All the concentrations have been normalised to the upper crust composition (Taylor and McLennan, 1995) (see supplementary materials Fig. SI-6). Compare to the upper crust reference, the suspended and bed load sediments are enriched in several elements in the order Sb >Pb>>> Cu, Sn, Zn, Cd >> Co, Fe, Cr, V. Compare to the bed load sediment, the suspended sediments present a significant enrichment in Cd >> Sn, Sb, Zn, Pb, > Co.

4. Discussion

4.1. Discharge-related variations of Cu concentration and isotopic composition at upstream sampling point of the Meca River

During the rain-free period and steady-state conditions, the low water discharge(< 0.5 m^3/s, field measurement using the "bucket" method) is associated with low pH and high copper (>100 mg/L) and other metals and sulphate concentrations in the dissolved phase (i.e., <0.22 µm) of the Meca River. An opposite tendency is observed during high rain and runoff. This behavior is consistent with the streamflow - sulphate concentration relationship defined by Galvan et al. (2009) (see chapter 2.2) and the fact that we observe in the present study a close relationship between Cu and sulphate concentrations (see Fig. 2). The upstream $\delta^{65}Cu$ values fluctuate significantly between -0.47 ‰ during high rainfall and -0.08 ‰ during low rainfall (see Fig. 4). For the low water discharge period, we assume that the Meca River is mainly fed by emptying lakes and galleries (groundwater) from the Tharsis mining district since the upstream point is the integrative water collection point of the whole mining district (Perez-Ostale, 2014). The close to zero values obtained during low water period therefore represent

351 the isotopic composition of water in direct contact with the sulfide-rich parent materials and
352 their host rocks.

353 The lower Cu concentrations (and other metals) obtained during the high water discharge
354 cannot be explained by a single dilution process by meteoric waters since Cu isotopic
355 composition drastically changed with time (Fig. 4). This implies that (an)other(s) source(s)
356 and/or process(s) contribute(s) to the flux of metals in the Meca River. We hypothesizsed that
357 the large amount of abandoned wastes ~~presents~~ within the Tharsis mining district of the Meca
358 River watershed could be a significant contributor during flood events. Indeed, Perez-Ostale
359 (2014) reported that more than 80 ha of wastes are present within the Tharsis mining district
360 without any remediation measures and thus represent a major source of elements (metals and
361 metalloids) during flood event. In the Lagunazo mine area (Iberian Pyrite Belt), negative
362 δ^{65}Cu value (-0.70 ± 0.04 ‰) has been reported for waters percolating through pyrite-rich
363 wastes (Viers et al., 2018). The Lagunazo mine, mined for copper, is constituted by a massive
364 sulfide deposit located North-West of the Tharsis deposit. If we consider this negative
365 signature as a first approximation of the average isotopic composition of waters percolating
366 through the abandoned wastes of the Tharsis mine plant, the leaching of waste during periods
367 of intense precipitation can induce a lower isotopic composition in the Meca River since this
368 river is the outlet of this mining area. In the event of rainfall and after prolonged dry period,
369 rain water quickly dissolves highly soluble sulphates or other secondary minerals that have
370 been deposited during the dry period within the wastes and in the major bed of the river
371 (Sanchez-Espana et al., 2005; Valente et al., 2013). The mineralogical study revealed the
372 presence of secondary minerals with characteristics of mine wastes (copiapite or jarosite type
373 minerals) but also the predominance of a muscovite type minerals suggesting also the
374 contribution of surrounding soils (see section 4.3).

We performed a mass-balance modelling to check if the isotopic composition of the Meca River at the upstream point could be explained by a mixing of waters originating from these two supposed main sources, lakes/galleries and leaching of abandoned wastes (Fig. 5). In this modelling, the isotopic compositions of waters percolating through the wastes varied from -0.45 to -1.95‰ with a Cu concentration set at 10 mg/L while the concentration and isotopic composition of Cu in galleries and lakes were set at 150 mg/L and -0.05 (δ^{65}Cu, in ‰), respectively. The isotopic signature used to characterise the "waste" pool was chosen to encompass the value obtained by Viers et al. (2018) (-0.70 ± 0.04 ‰) for waters percolating through pyrite-rich wastes. Additional theoretical curve with δ^{65}Cu of -1.95% was required to encompass the upstream points at intermediate concentrations of dissolved Cu (Fig. 5). It can be seen that, while open mine lakes are the major source of riverine Cu during dry periods, their role becomes minor during flood.

Another process that could interfere in the resulting isotopic composition of the Meca River at the upstream point is precipitation of secondary minerals within the main stem. Indeed, the upstream waters are slightly oversaturated with respect to jarosite ($KFe_3(SO_4)_2(OH)_6$), goethite (FeOOH), and a cupric ferrite type mineral ($CuFe_2O_4$) (see Fig. 6). It has been previously shown that goethite, jarosite and schwertmannite could precipitate at the pH of 2 to 3 in the river water (Sanchez Espana et al., 2005).As the suspended matter and bed load sediment were enriched in lighter isotopes ($\delta^{65}Cu_{suspended\text{-}matter}$= -0.41 ± 0.03 ‰; $\delta^{65}Cu_{sediment}$ = -1.92 ± 0.04 ‰), the minerals precipitation can exert strong effect on the isotopic composition of the river water. For example, precipitation of isotopically-light solid phases will enrich the river water in heavier isotopes via mass balance effect. Copper exhibited heavier isotopic composition during low flow period but the effect cannot be quantitatively assessed. However, the absence of copper in the form of small colloids (see section 4.2) would suggest a source change rather than a process within the water column to

explain the variation in isotopic composition. Indeed, the precipitation of secondary minerals should take place via precursors and in particular the presence of colloidal particles.

Overall, based on diel cycle under contrasting hydrological regime in the upstream point, Cu isotopes allowed us to detect two distinct sources of Cu in the river, which are: *i)* lake water under dry conditions, and *ii)* a mix of lake and soil/waste deposit runoff sources under flood conditions. A multi-parametric statistical treatment suggests that the data structure is governed by one single factor that could be related to the water discharge. With the exception of Na and K, all elements exhibit a temporal pattern which is similar to that of Cu.

4.2 Variations of Cu concentration and isotopic composition at the downstream sampling point of the Meca River

Located 20 km down from the upstream sampling point, the downstream point exhibits much lower dissolved Cu concentrations (~0.28 mg/L to ~1.6 mg/L).With δ^{65}Cu values ranging from -0.63 ± 0.03‰ (2σ) to -0.29 ± 0.02‰ (2σ), downstream sampling point exhibits both narrower and negative values compared to upstream during the same sampling period (Fig. 4A and 4B).

Because of the lack of hydrological data for both Meca River and tributaries it was impossible for us to physically constrain the mixing processes. Consequently, we will discuss qualitatively the processes that may affect the isotopic composition between the upstream and the downstream points.

A dilution of mine waters by tributaries and lateral input through soils of the watershed are primarily responsible for Cu isotope evolution over the Meca River watercourse. The lighter isotopic composition of the downstream point could result from direct contribution of the Meca tributaries through a dilution process. We sampled only one of these tributaries which

425 exhibited low Cu concentration (0.3 mg/L) and light isotopic composition ($\delta^{65}Cu_{tributary}$ = -
426 2.72 ± 0.03 ‰). As this Meca tributary is draining non mining plant zone, we suggest our
427 sampling to be representative of the soil catchment contribution between the mine district and
428 the downstream sampling point. A small fraction of this Cu could be natural Cu originating
429 from the chemical weathering of the parental rocks that have an average value of 55 mg/kg
430 (Chopin and Alloway, 2007). A more significant fraction of Cu present in the surrounding
431 soils may originate from the mine after deposition of atmospheric particles on these soils.
432 Indeed, smelting activity was conducted on the Tharsis site for many years (Valente et a.,
433 2013) and Chopin and Alloway (2007) have revealed that in the case of Tharsis, the soils
434 appear to be contaminated significantly in the vicinity of the mine (2 to 3 km around). As
435 copper presents a strong affinity for organic matter, organic (O) soil horizons are generally
436 enriched in copper with respect to deepest soil horizons (Bigalke et al., 2011), what was
437 observed by Chopin and Alloway (2007). Based on a mass balance calculation,

438 $$(\delta^{65}Cu \times [Cu])_{downstream} = (\delta^{65}Cu \times [Cu])_{tribute\_stream} + (\delta^{65}Cu \times [Cu])_{upstream}$$

439 where [Cu] stands for Cu concentration, we estimated that 87 % of the downstream Cu comes
440 from the upstream point, and only 13% from the tributary streams.

441 In this case, it seems that only inputs of tributaries with exogenous Cu would be able to
442 affect $\delta^{65}Cu$ downstream values.

443 Furthermore, during the water flow between the mine/upstream and downstream point,
444 various in-stream processes could control Cu concentration and isotopic composition in the
445 fluid. These are: i) precipitations of secondary Cu-bearing minerals; ii) Cu sorption onto
446 major mineral phases of river bed sediments; iii) Cu uptake by aquatic microorganisms. These
447 processes are likely to be mostly pronounced in the downstream point, given that highly
448 acidic upstream waters (pH = 2.4 to 2.8) are not favourable for adsorption and biota

449 development. At the downstream point, speciation calculations show that the fluid is largely
450 oversaturated with respect to schwertmannite ($Fe_8O_8(SO_4)_x(OH)_y,nH_2O$), a cuprite type
451 mineral ($CuFe_2O_4$) and at a lesser extent jarosite ($KFe_3(SO_4)_2(OH)_6$), goethite (FeOOH) and
452 ferrihydrite ($Fe_2O_3,0.5H_2O$) (see Fig. 6). Within the AMD context, it is known that the
453 heavier Cu isotopic composition of the solution with respect to that of bulk chalcopyrite could
454 be due to the precipitation of an isotopically light Cu-rich solid phase (Kimball et al., 2009).
455 More recent work suggested that the progressive enrichment of Cu heavier isotope along the
456 Cobica River, draining the Lagunazo copper mine, could be due to the precipitation of some
457 secondary minerals enriched in light isotopes (Viers et al., 2018). The values obtained for
458 suspended and bed sediments of the Meca River ($\delta^{65}Cu_{susp\text{-}sed}$ = –0.41 ± 0.03 ‰ and
459 $\delta^{65}Cu_{sediment}$ = –1.92 ± 0.04 ‰) seem to support this assumption since the secondary products
460 are enriched in light isotopes. However, given that the isotopic composition at the
461 downstream point (–0.29 to –0.63‰) is globally lower than that at the upstream point (–0.08
462 to –0.47‰), we suggest that secondary mineral precipitation cannot be sole process controlling
463 Cu isotope fractionation, and other mechanisms should be considered.

464 The higher pH measured at the downstream point (3.61 to 5.68) compared to the upstream
465 point (2.41 to 2.82) implies a possibility of metals sorption onto the surface of suspended
466 sediments in the course of the water flow, as it is known for other mine water-affected
467 environments (Lee et al., 2002; Smith, 1999). We identified the presence of Fe oxides and
468 other (hydr)oxide minerals in the suspended matter of the Meca River (see section 4.3) that
469 can offer substantial surfaces for Cu sorption. Balistrieri et al. (2008) and Pokrovsky et al.
470 (2008) have shown that Cu sorption onto common mineral and organic surfaces favors the
471 heavy isotope leaving isotopically light Cu in the aqueous solution. The effect of the sorption
472 process could not be quantified but is consistent with a lower isotopic composition in the
473 downstream point.

Finally, third mechanism affecting Cu isotope composition in the river water is Cu interaction with aquatic microorganisms. During our sampling period, the temperature was low (13.6 – 17.1°C, upstream) and we did not detect any algal bloom that could have affected the dissolved Cu. Moreover, the uptake of Cu by bacteria, peryphytic biofilm or algae favors the light Cu isotope into the biomass (Navarette et al. 2011; Coutaud et al., 2018). This process would enrich the river water in heavy isotope, which is not consistent with our observations.

5. Conclusions

This study presented both Cu concentration and isotopic composition of the Meca River draining one of the largest abandoned mine of the Iberian Pyrite Belt during a flood event. Based on observations over the diel cycle under changing water regime conditions, Cu isotopes are useful to understand the hydrochemical functioning of a complex mining zone. In response to a change in the hydrological conditions, the system appears to react quickly since Cu isotopic composition changes following the amount of precipitation/water discharge in the mining area. In the case of the Tharsis mine, copper isotopes allowed us to detect two distinct metal sources in the headwater catchment under constrained hydrological regime. A major contribution was provided by lake/gallery source under dry conditions, whereas during the flood, a mix of lake/gallery and soil/waste deposit contributed to lateral surface runoff. These findings could be useful for mine remediation measures and monitoring practices. Twenty km downstream the mine, the Cu isotopic composition is essentially controlled by a dilution and mixing process of headwater catchment by lateral surface runoff within soils brought by tributaries. It is not strongly modified by in-stream environmental processes such as

precipitation of Cu secondary bearing minerals, sorption on mineral surfaces or uptake by aquatic organisms.

Acknowledgments

This work was supported by the EC2CO program of the INSU/CNRS institution and by the European Union for co-funding SOIL TAKE CARE SOE1/P4/F0023 through the European Regional Development Fund (ERDF), under the Interreg SUDOE Program. This work was also partly supported by the EQUIPEX CRITEX programme (grant no. ANR-11-EQPX-0011, Pls. J. Gaillardet and L. Longuevergne). We deeply thank Ludovic Menjot and Priscia Oliva for their technical and scientific help in XRD data acquisition and interpretation, Manuel Henry for his help in the clean room, and Stéphanie Mounic for anions concentrations measurements at the GET laboratory. We want to also express our gratitude to our Stéphane Le Blond du Plouy from the Centre de MicroCaractérisation Raimond Castaing for his technical support in SEM-EDX characterisation. We would also like to thank the staff of the management department without which nothing could be achieved. The reviewers should be deeply thanked for their work.

References:

Abdi, H. 2010. Partial least squares regression and projection on latent structure regression (PLS Regression). Wiley Interdisciplinary Reviews: Computational, https://doi.org/10.1002/wics.51

Achterberg E.P., Herzl V.M.C., Braungardt C.B., Millward G.E., 2003. Metal behaviour in an estuary polluted by acid mine drainage: the role of particulate matter. Environ. Pollut. 121, 283-292.

Almodovar,, G. R., Castro, J. A., Sobol, F., Toscano, , M., 1997. Geology of the Riotinto Ore Deposits, Geology and VMS deposits of the Iberian Pyrite Belt. SEG Fieldbook Series, Society Economic Geologists, Volume 27, p. 165-172.

Balistrieri, L.S., Borrok, D.M., Wanty, R.B., Ridley, W.I., 2008. Fractionation of Cu and Zn isotopes during adsorption onto amorphous Fe (III) oxyhydroxide: experimental mixing of acid rock drainage and ambient river water. Geochim. Cosmochim. Acta 72(2), 311-328.

Bigalke, m., Weyer, S., Wilcke, W., 2011. Stable Cu istope fractionation in soils during oxic weathering and podzolization. Geochim. Cosmochim. Acta 75, 3119-3134.

Bigham, J.M., Schwertmann, U., Traina, S.J., Winland, R.L., Wolf, M., 1996. Schwertmannite and the chemical modeling of iron in acid sulfate waters. Geochim. et Cosmochim. Acta 12, 2111-2121.

Blondet I., Schreck E., Viers J., Casas S., Jubany I., Bahi N., Zouiten C., Dufréchou G., Freydier R., Galy-Lacaux C., Martinez-Martinez S., Faz A., Soriano-Disla M., Acosta J.A., Darrozes J., 2019. Atmospheric dust characterisation in the mining district of Cartagena-La Unión, Spain: Air quality and health risks assessment. Sci. Tot. Environ. 693, 133496.

536 Blotevogel S., Oliva P., Sobanska S., Viers J., Vezin H., Audry S., Prunier J., Darrozes J., Orgogozo
537 L., Courjault-Radé P., Schreck E., 2018. The fate of Cu pesticides in vineyard soils: A case
538 study using δ 65 Cu isotope ratios and EPR analysis. Chem. Geol. 477, 35-46.
539 Borrok, D.M., Nimick, D.A., Wanty, R.B., Ridley, W.I., 2008. Isotopic variations of dissolved copper
540 and zinc in stream waters affected by historical mining. Geochim. Cosmochim. Acta 72(2),
541 329-344.
542 Chopin, E., Alloway, B., 2007. Distribution and mobility of trace elements in soils and vegetation
543 around the mining and smelting areas of Tharsis, Riotinto and Huelva, Iberian Pyrite Belt, SW
544 Spain. Water, Air, and Soil Pollut., 182(1-4), 245-261.
545 Conde, C., Tornos, F., Large, R., Danyushevsky, L., Solomon, M., 2009. Análisis de elementos traza
546 por la LA-ICPMS en pirita de los sulfuros masivos de Tharsis (FPI). Macla, 63–64.
547 Coutaud M., Meheut M., Glatzel P., Pokrovski G.S., Viers J., Rols J-L., Pokrovsky O.S., 2018. Small
548 changes in Cu redox state and speciation generate large isotope fractionation during
549 adsorption and incorporation of Cu by a phototrophic biofilm. Geochim. Cosmochim. Acta
550 220, 1-18.
551 Dótor-Almazán, A., Armienta-Hernández, M.A., Talavera-Mendoza, O., Ruiz, J., 2017. Geochemical
552 behavior of Cu and sulfur isotopes in the tropical mining region of Taxco, Guerrero (southern
553 Mexico). Chem. Geol., 471, 1-12.
554 Dupré B., Viers J., Dandurand J-L., Polvé M., Bénézeth P., Vervier P., Braun J-J., 1999. Major and
555 trace elements associated with colloids in organic-rich river waters: Ultrafiltration of natural
556 and spiked solutions. Chem. Geol. 160, 63-80.
557 Elbaz-Poulichet, F., Braungardt, C., Achterberg, E., Morley, N., Cossa, D., Beckers, J., Nomérange,
558 P., Cruzado, A., Leblanc, M., 2001. Metal biogeochemistry in the Tinto–Odiel Rivers
559 (Southern Spain) and in the Gulf of Cadiz: a synthesis of the results of TOROS project. Cont.
560 Shelf Res. 21 (18–19), 1961–1973.
561 Fernandez, A., Borrok, D.M., 2009. Fractionation of Cu, Fe, and Zn isotopes during the oxidative
562 weathering of sulfide-rich rocks. Chem. Geol.,, 264(1-4), 1-12.
563 Galvan L., Olias M., Fernandez de Villaran R., Domingo Santos J-M., Nieto J-M., Sarmiento A-M.,
564 Canovas C.R., 2009. Aplication of the SWAT model to an AMD-affected River (Meca River,
565 SW Spain). Estimation of transported pollutant load. J. Hydrol. 377, 445-454.
566 Grande J-A., de la Torre M-L., Céron J-C., Beltran R., Gomez T., 2010. Overall hydrochemical
567 characterization of the Iberian Pyrite Belt. Main acid mine drainage-generating sources
568 (Huelva, Spain). J. Hydrol. 390, 123-130.
569 Grande, J.A., Santisteban, M., De la Torre, M., Valente, T., Pérez-Ostalé, E., 2013. Characterisation of
570 AMD pollution in the reservoirs of the Iberian Pyrite Belt. Mine Water Environ.32(4), 321-
571 330.
572 Grande, J-A., Santisteban M., de la Torre, M.L., Davila, J.M., Perez-Ostalé E., 2018. Map of impact
573 by acid mine drainage in the river network of The Iberian Pyrite Belt (Sw Spain).
574 Chemosphere 199, 269-277.
575 Kimball, B.E., Mathur, R., Dohnalkova, A.C., Wall, A.J., Runkel, R.L., Brantley, S.L., 2009. Copper
576 isotope fractionation in acid mine drainage. Geochim. et Cosmochim. Acta 73, 1247-1263.
577 Leblanc, M., Morales, J., Borrego, J., Elbaz-Poulichet, F., 2000. 4,500-year-old mining pollution in
578 southwestern Spain: long-term implications for modern mining pollution. Econ. Geol. 95(3),
579 655-662.
580 Lee, G., Bigham, J.M., Faure, G., 2002. Removal of trace metals by coprecipitation with Fe, Al and
581 Mn from natural waters contaminated with acid mine drainage in the Ducktown Mining
582 District, Tennessee. Appl. Geochem. 17(5), 569-581.
583 Marechal, C. N., P. Telouk, Albarède F., 1999. Precise analysis of copper and zinc isotopic
584 compositions by plasma-source mass spectrometry. Chemical Geology 156(1-4): 251-
585 273.
586 Mathur, R., Ruiz, J., Titley, S., Liermann, L., Buss, H., Brantley, S., 2005. Cu isotopic fractionation in
587 the supergene environment with and without bacteria. Geochim. Cosmochim. Acta 69(22),
588 5233-5246.

589 Mathur, R., Titley, S., Barra, F., Brantley, S., Wilson, M., Phillips, A., Munizaga, F., Maksaev, V.,
590 Vervoort, J., Hart, G., 2009. Exploration potential of Cu isotope fractionation in porphyry
591 copper deposits. J. Geochem. Explor. 102, 1-6.
592 Mathur, R., Munk, L.A., Townley, B., Gou, K.Y., Gomez Miguelez, N., Titley, S., Chen, G.G., Song,
593 S., Reich, M., Tornos, F., Ruiz, J., 2014. Tracing low-temperature aqueous metal migration in
594 mineralized watersheds with Cu isotope fractionation. Appl. Geochem. 51, 109-115.
595 Moreno-Gonzalez R., Canovas C.R., Olias M., Macias F., 2020. Seasonal variability of extremely
596 metal rich acid mine drainages from the Tharsis mine (SW Spain). Environ. Pollut. 259,
597 113829.
598 Navarrete, J.U., Borrok, D.M., Viveros, M., Ellzey, J.T., 2011. Copper isotope fractionation during
599 surface adsorption and intracellular incorporation by bacteria. Geochim. Cosmochim. Acta 75,
600 784-799.
601 Nieto, J.M., Sarmiento, A.M., Olias, M., Canovas, C.R., Riba, I., Kalman, J., Delvalls, T.A., 2007.
602 Acid mine drainage pollution in the Tinto and Odiel rivers (Iberian Pyrite Belt, SW Spain) and
603 bioavailability of the transported metals to the Huelva Estuary. Environ. Int. 33(4), 445-455.
604 Nimick, D.A., Gammons, C.H., Parker, S.R., 2011. Diel biogeochemical processes and their effect on
605 the aqueous chemistry of streams: A review. Chem. Geol. 283, 3-17.
606 Olias M., Canovas C.R., Basallote M.D., Macias F., Perez-Lopez R., Moreno-Gonzalez R., Millan-
607 Becerro R., Nieto J.M., 2019. Causes and impacts of a mine water spill from an acidic pit lake
608 (Iberian Pyrite Belt). Environ. Pollut. 250, 127-136.
609 Pérez Ostalé, E., 2014. Caracterización ambiental de estructuras mineras en la Faja Pirítica Ibérica
610 como soporte metodológico de gestión territorial. Tesis doctoral, Universidad de Huelva,
611 Spain.
612 Perez Rodriguez, N., Engström, E., Rodushkin, I., Nason, P., Alakangas, L., Öhlander, B., 2013.
613 Copper and iron isotope fractionation in mine tailings at the Laver and Kristineberg mines,
614 northern Sweden. Appl. Geochem. 32, 204-215.
615 Petit, J. C. J., de Jong, J., Chou, L., Mattielli, N. (2008). Development of Cu and Zn Isotope
616 MC-ICP-MS Measurements: Application to Suspended Particulate Matter and
617 Sediments from the Scheldt Estuary. Geostandards and Geoanalytical Research 32(2),
618 149-166.
619 Pokrovsky O., Viers J., Emnova E.E., Kompantseva E.I., Freydier R., 2008. Copper isotope
620 fractionation during its interaction with soil and aquatic microorganisms and metal
621 oxy(hydr)oxides: possible structural control. Geochim. et Cosmochim. Acta 72, 1742-1757.
622 Roebbert, Y., Rabe, K., Lazarov, M., Schuth, S., Schippers, A., Dold, B., Weyer, S., 2018.
623 Fractionation of Fe and Cu isotopes in acid mine tailings: Modification and application of s
624 sequential extraction method. Chem. Geol. 493, 67-79.
625 Sáez R., Pascual E, Toscazo M. y Almodovar G. R., 1999. The Iberian type of volcanosedimentary
626 massive sulphide deposits. Miner. Depos. 34, 549-570.
627 Sainz, A., Grande, J., De la Torre, M., 2004. Characterisation of heavy metal discharge into the Ria of
628 Huelva. Environ. Int. 30(4), 557-566.
629 Sanchez Espana J., Lopez Pamo E., Santofimia Pastor E., Reyes Andrés J., Martin Rubi J-A., 2005.
630 The natural attenuation of two acidic effluents in Tharsis and La Zarza-Perrunal mines
631 (Iberian Pyrite Belt, Huelva, Spain). Environ. Geol. 49, 253-266.
632 Sanchez-Espana J., Yusta I., Diez-Ercilla M., 2011. Schwertmannite and hydrobasaluminite : A re-
633 evaluation of their solubility and control on the iron and aluminium concentration in acidic pit
634 lakes. Appl. Geochem. 26, 1752-1774.
635 Santisteban Fernandez M. (2015). Incidencia de procesos AMD en la hidroquimica de embalses
636 afectados en la faja piritica ibérica. Thesis, Universidad de Huelva.
637 Sarmiento A.M., Nieto, J.M., Olias, M., Canovas, C.R., 2009a. Hydrochemical characteristics and
638 seasonal influence on the pollution by acid mine drainage in the Odiel River basin (SW Spain).
639 Appl. Geochem. 24, 697-714.
640 Sarmiento, A.M., Olias, M., Nieto, J.M., Canovas, C.R., Delgado J., 2009b. Natural attenuation
641 processes in two water reservoirs receiving acid mine drainage. Sci. Total Environ. 407, 2051-
642 2062.

643 Smith, K.S., 1999. Metal sorption on mineral surfaces: an overview with examples relating to mineral
644 deposits. The environmental geochemistry of mineral deposits. Rev. Eco. Geol. 6, 161-182.
645 Song, S., Mathur, R., Ruiz, J., Chen, D., Allin, N., Guo, K., & Kang, W., 2016. Fingerprinting two
646 metal contaminants in streams with Cu isotopes near the Dexing Mine, China. Sci. Total
647 Environ. 544, 677-685.
648 Teng, F.-Z., Dauphas, N., Watkins, J.M., 2017. Non-traditional stable isotopes: retrospective and
649 prospective. Rev. Mineral. Geochem. 82(1): 1-26.
650 Taylor, S.R., MacLennan, S.M. 1985. The Continental Crust: its Composition and Evolution.
651 Blackwell, Oxford (312 pp.).
652 Tornos, F., Solomon, M., Conde, C., Spiro, B., 2008. Formation of the Tharsis massive sulfide
653 deposit, Iberian Pyrite Belt: geological, lithologeochemical, and stable isotope evidence for
654 deposition in a brine pool. Econ. Geol. 103, 185–214.
655 Valente, T., Grande, J., De La Torre, M., Santisteban, M., Cerón, J., 2013. Mineralogy and
656 environmental relevance of AMD-precipitates from the Tharsis mines, Iberian Pyrite Belt
657 (SW, Spain). Appl. Geochem. 39, 11-25.
658 Vasyukova E.V., Pokrovsky O.S., Viers J., Oliva P., Dupré B., Martin F., Candaudap F., 2010. Trace
659 elements in organic- and iron-rich surficial fluids of the boreal zone : Assessong colloidal
660 forms via dialysis and ultrafiltration. Geochim. et Cosmochim. Acta 74(2), 449-468.
661 Viers J., Dupré B., Polvé M., Schott J., Dandurand J-L., Braun J-J., 1997. Chemical weathering in the
662 drainage basin of a tropical watershed (Nsimi-Zoétélé site, Cameroon): comparison between
663 organic-poor and organic rich waters. Chem. Geol. 140, 181-206.
664 Viers, J., Grande, J.A., Zouiten, C., Freydier R., Masbou, J., Valente, T., de la Torre M-L.,
665 Destrigneville, C., Pokrovsky, O.S., 2018. Are Cu isotopes a useful tool to trace metal sources
666 and processes in acid mine drainage (AMD) context? Chemosphere, 193, 1071-1079.
667 Viollier E., Inglett P.W., Hunter K., Roychoudhury, Van Cappellen P., 2000. The ferrozine method
668 revisited : Fe(II)/Fe(III) determination in natural waters. Appl. Geochem. 15, 785-790.
669 Wold, H. 1985. Partial Least Squares. In: Kotz, S. and Johnson, N.L., Eds., Encyclopedia of Statistical
670 Sciences, Vol. 6, John Wiley, New York, 581-591
671

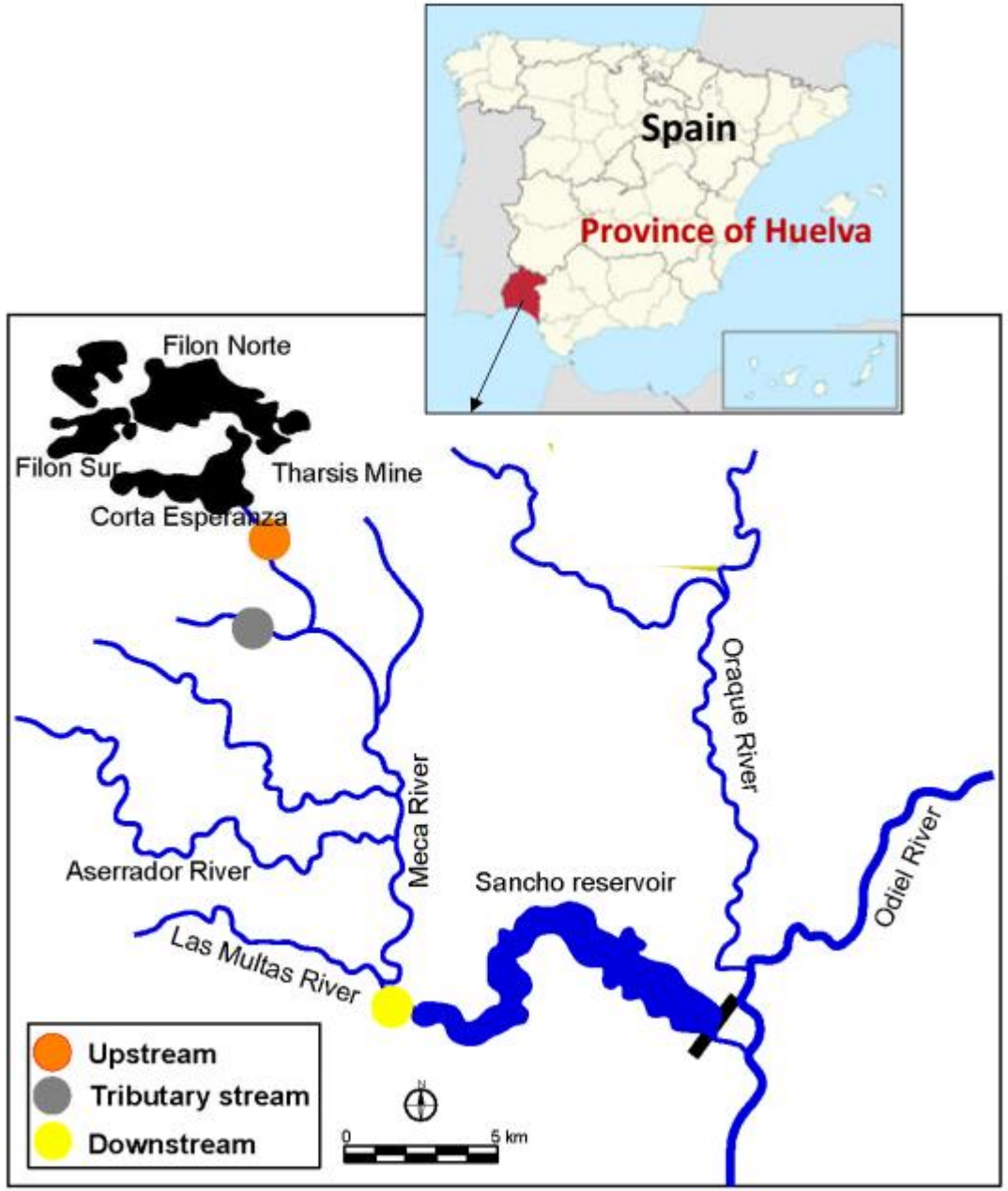

Fig. 1: Upstream, tributary stream and downstream sampling locations within the Meca River. The Meca River is a tributary of the Odiel River (Huelva, Spain).

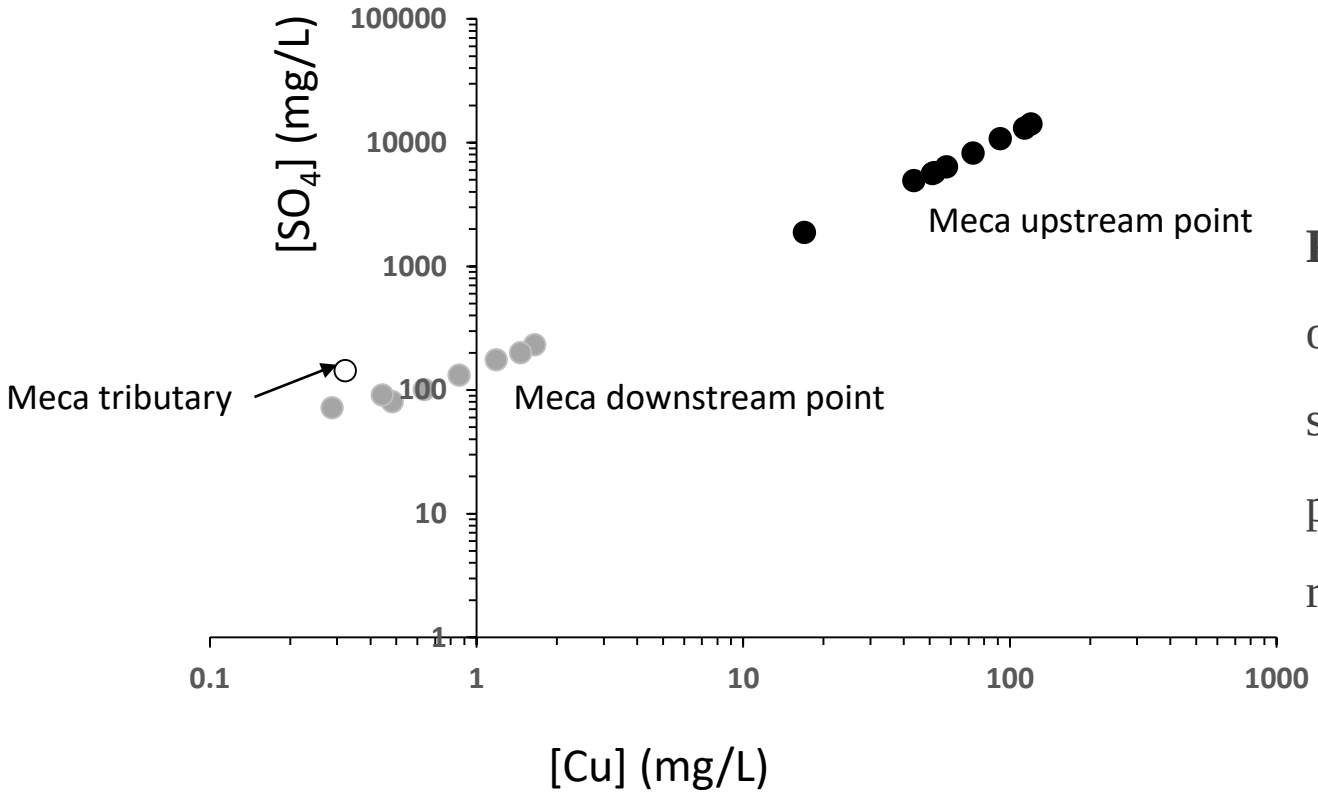

Figure 2: Dissolved Cu concentration as a function of SO_4^{2-} concentrations for upstream (black symbols) and downstream (gray symbols) sampling points of the Meca River. The Meca tributary is also reported.

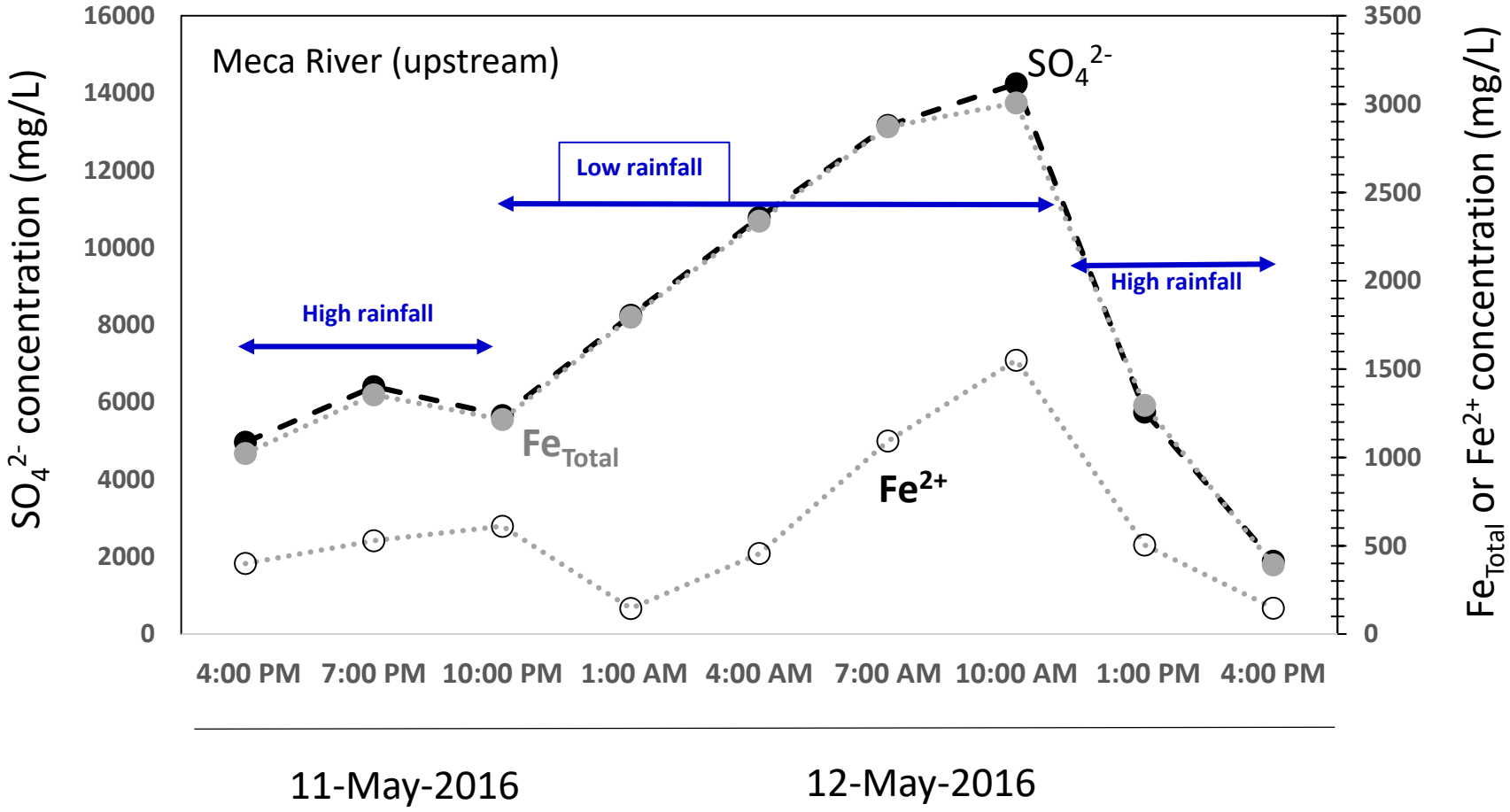

Figure 3: Dissolved SO_4^{2-} concentrations as a function of dissolved iron (Total and Fe^{2+}) concentrations for upstream sampling points of the Meca River.

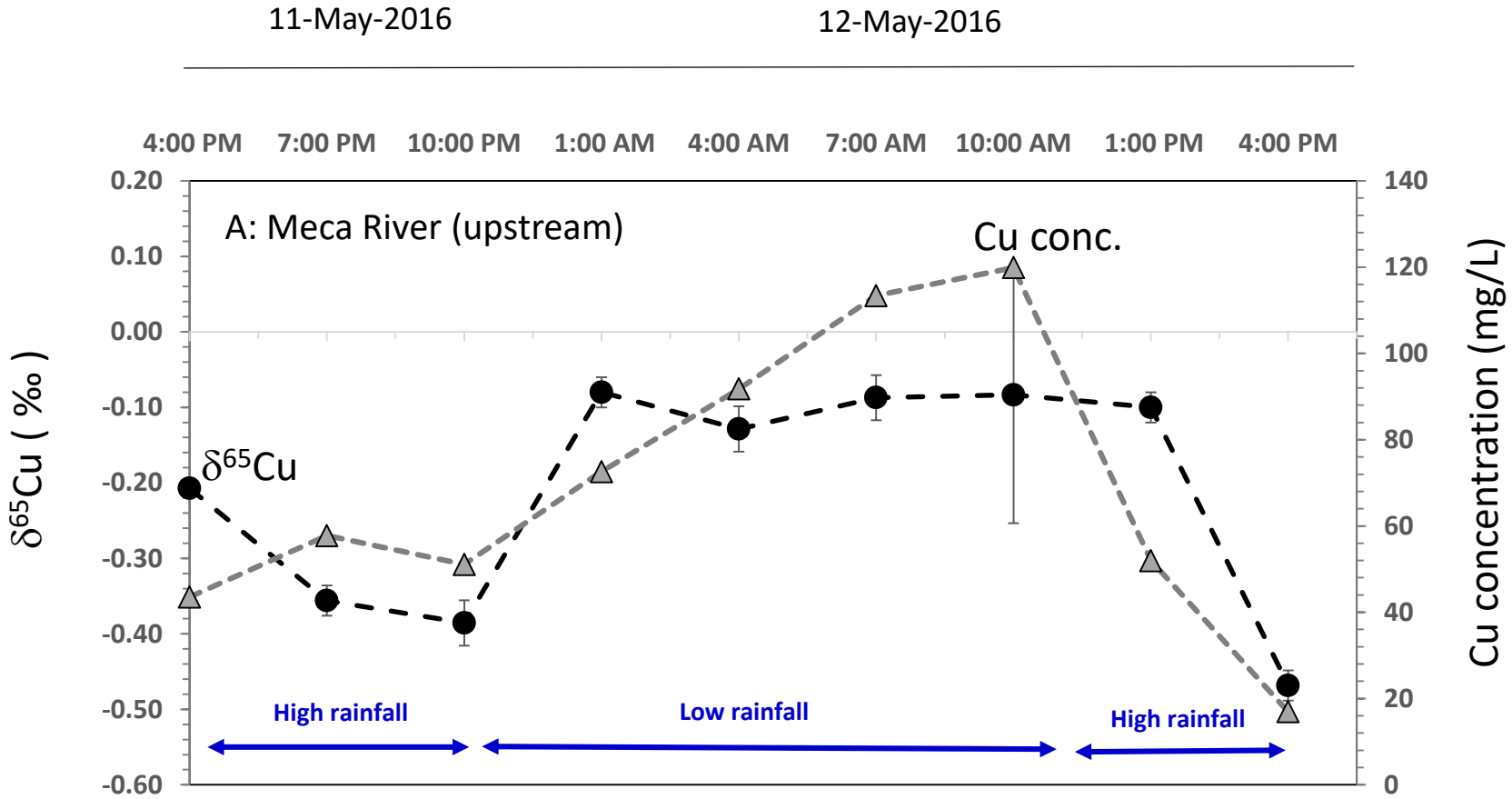

Figure 4: Diel variation in $\delta^{65}Cu$ (left axis, black circle) and dissolved Cu concentrations (right axis, gray triangle) for A) upstream and B) downstream. Error bars represent 2σ uncertainties calculated from replicate analyses.

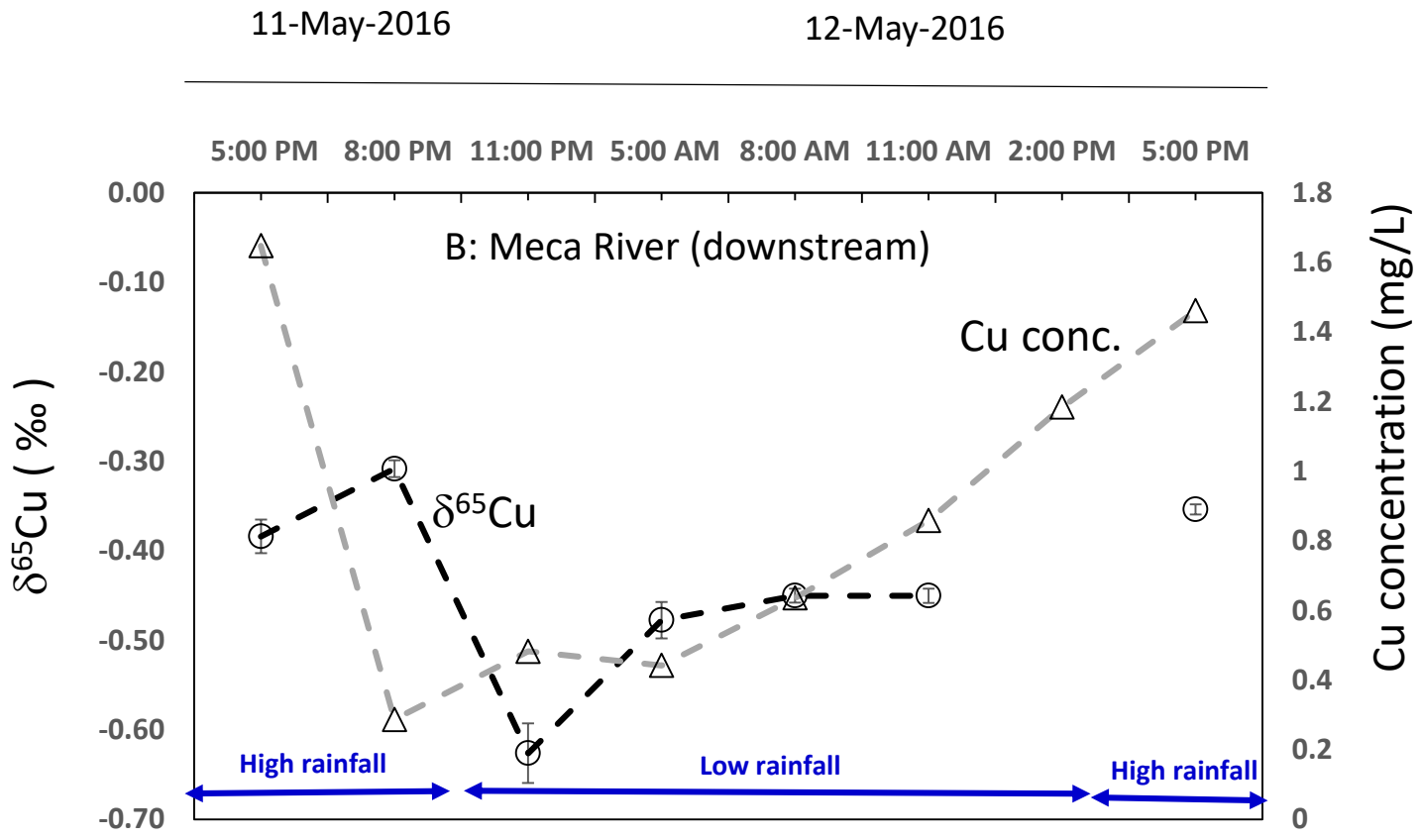

Figure 4 (to be continued)

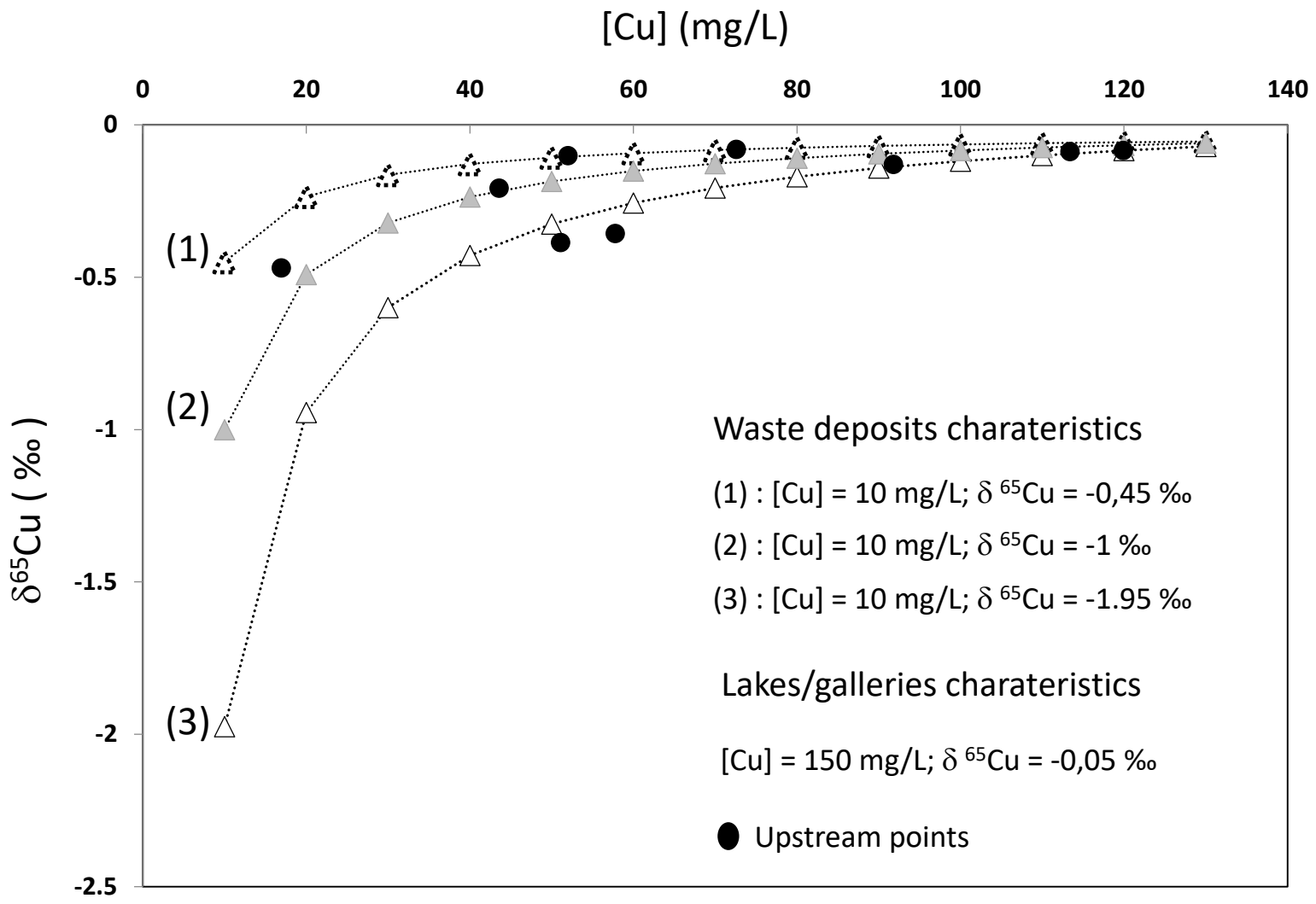

Figure 5: Theoretical mixing diagram between 1) water percolating through the wastes deposits and 2) water originating from the mine lakes and galleries The black points are the values measured for the upstream sampling point.

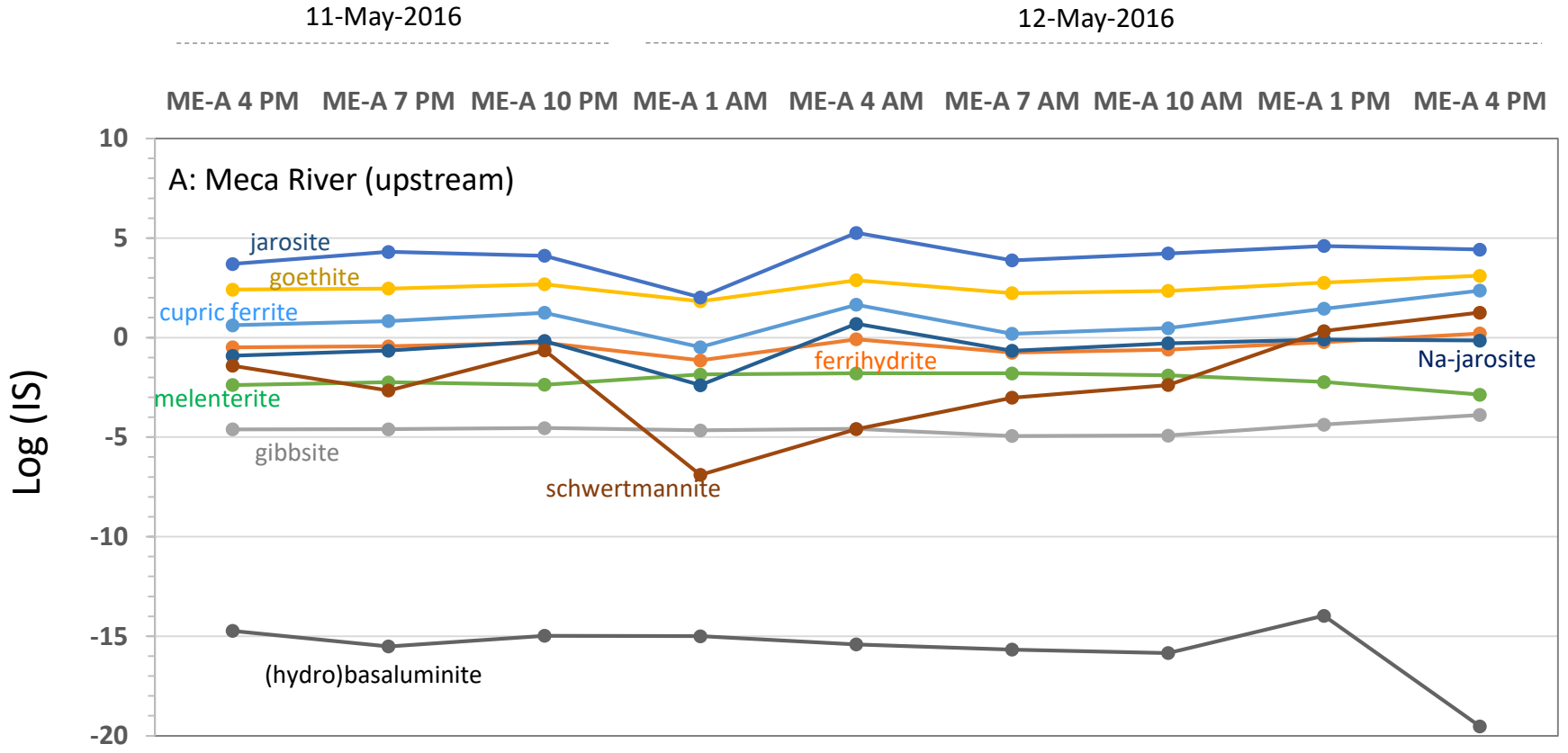

Figure 6: Saturation indexes calculated using Visual MINTEQ ver. 3.0. at both upstream and downstream sampling points of the Meca River.

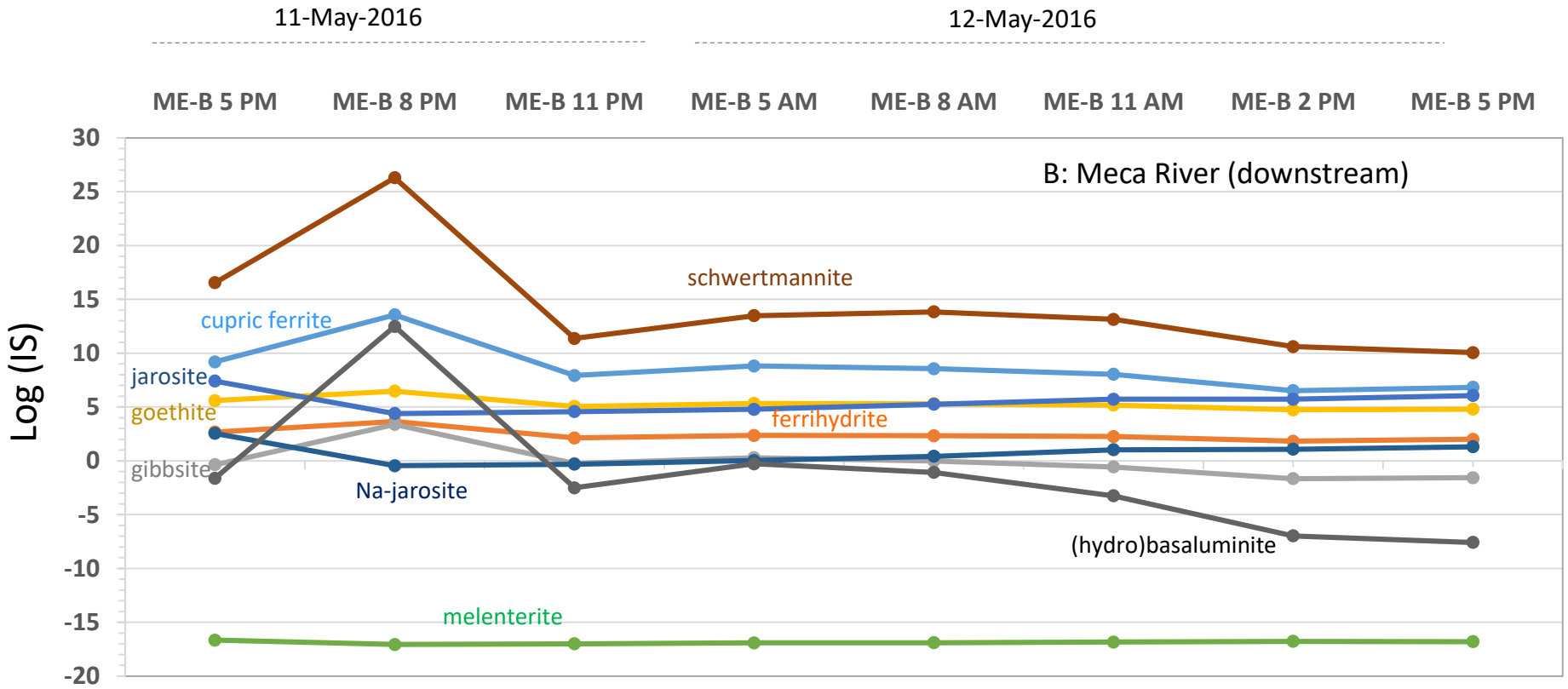

Figure 6: (to be continued)

Sampling date		11-May-2016	11-May-2016	11-May-2016	11-May-2016	11-May-2016	12-May-2016	12-May-2016	12-May-2016	12-May-2016	12-May-2016	12-May-2016	12-May-2016	12-May-2016	11-May-2016	11-May-2016	11-May-2016	11-May-2016	12-May-2016	12-May-2016	12-May-2016	12-May-2016	12-May-2016
Sampling name		ME-A 4:00 PM	ME-A 4:00 PM	ME-A 7:00 PM	ME-A 10:00 PM	ME-A 10:00 PM	ME-A 1:00 AM	ME-A 4:00 AM	ME-A 4:00 AM	ME-A 7:00 AM	ME-A 10:00 AM	ME-A 10:00 AM	ME-A 1:00 PM	ME-A 4:00 PM	ME-A AFL	ME-B 5:00 PM	ME-B 8:00 PM	ME-B 11:00 PM	ME-B 5:00 AM	ME-B 8:00 AM	ME-B 11:00 AM	ME-B 2:00 PM	ME-B 5:00 PM
Filtration size		<0,22 µm	<1000 da	<0,22 µm	<0,22 µm	<1000 da	<0,22 µm	<0,22 µm	<1000 Da	<0,22 µm	<0,22 µm	<1000 Da	<0,22 µm	<0,22 µm	<0,22 µm	<0,22 µm	<0,22 µm	<0,22 µm	<0,22 µm	<0,22 µm	<0,22 µm	<0,22 µm	<0,22 µm
	Unit																						
Temperature (°C)	°C	16,6	-	17,1	15,4	-	14,3	14,3	-	13,8	15,0	-	13,6	17,0	15,7	16,6	19,7	16,2	14,4	14,4	15,6	16,7	21,0
pH		2,60	-	2,52	2,57	-	2,56	2,50	-	2,43	2,41	-	2,64	2,82	3,85	4,12	5,68	4,27	4,52	4,34	4,09	3,69	3,61
Conductivity	mS/cm (at 25°C)	5,48	-	6,44	6,12	-	8,02	9,76	-	11,39	11,6	-	6,22	2,81	0,51	0,43	0,31	0,31	0,31	0,38	0,39	0,54	0,50
O_2	mg/L	6,46	-	6,30	6,61	-	6,64	6,45	-	6,54	6,48	-	8,4	7,65	6,94	-	-	-	-	-	-	-	-
DOC	mg/L	7,348	-	16,43	7,384	-	13,58	12,7	-	5,676	5,468	-	10,22	9,917	35,93	-	-	-	-	-	-	-	-
Cl	mg/L	10,67	-	11,61	11,12	-	11,98	12,85	-	13,80	14,07	-	8,85	8,28	21,84	25,03	29,11	26,29	30,19	26,89	26,76	27,69	17,32
NO_3	mg/L	1,07	-	0,95	1,09	-	1,19	1,08	-	1,01	0,84	-	0,80	1,25	34,74	1,93	1,88	2,12	2,26	1,65	1,74	1,89	3,09
SO_4	mg/L	4964	-	6407	5657	-	8251	10784	-	13163	14241	-	5746	1886	144	233	72	81	91	101	132	177	201
$\delta^{65}Cu$ (‰)		-0,21 (± 0.00)	-	-0,36 (± 0.02)	-0,39 (± 0.02)	-	-0,08 (± 0.03)	-0,13 (± 0.16)	-	-0,09 (± 0.02)	-0,08 (± 0.17)	-	-0,10 (± 0.02)	-0,47 (± 0.02)	-2,72 (± 0.03)	-0,38 (± 0.02)	-0,31 (± 0.01)	-0,63 (± 0.03)	-0,48 (± 0.02)	-0,45 (± 0.01)	-0,45 (± 0.01)		-0,35 (± 0.01)
Cu	mg/L	43,55	44,60	57,76	51,07	49,79	72,58	91,79	92,84	113,38	119,88	116,80	51,97	16,92	0,32	1,65	0,29	0,48	0,44	0,64	0,86	1,18	1,46
Na (mg/L)	mg/L	12,24	8,06	18,61	8,63	8,61	8,72	10,90	9,41	10,34	10,02	9,22	7,41	6,80	17,11	14,18	16,22	14,28	15,43	15,06	14,97	15,42	10,85
Mg (mg/L)	mg/L	267	256	334	282	283	419	530	549	672	723	693	313	91	16	17	10	9	10	11	12	14	14
Al (mg/L)	mg/L	298	283	358	317	319	468	602	628	775	826	799	360	101	3	12	1	3	2	4	6	8	10
Si (mg/L)	mg/L	16,04		20,12	18,12		22,56	25,06		27,63	29,33		14,33	8,54	5,29	4,95	4,12	4,03	4,31	4,77	-	5,19	5,51
K (mg/L)	mg/L	1,22	1,11	2,71	0,54	1,31	0,67	0,97	1,02	0,92	0,88	1,11	1,27	1,11	3,38	2,05	2,38	2,20	1,87	1,73	1,72	1,66	1,84
Ca (mg/L)	mg/L	54,10	47,81	100,17	54,25	51,10	70,70	85,65	86,89	106,17	112,66	108,95	50,72	19,05	21,92	10,49	9,81	8,56	8,96	8,90	9,34	10,04	9,48
Mn (mg/L)	mg/L	34,01	33,16	42,28	36,49	35,05	51,94	65,61	65,34	80,08	84,27	82,53	37,43	11,93	1,67	1,56	0,73	0,72	0,62	0,80	1,01	1,27	1,53
Fe (total)	mg/L	1023	1029	1355	1214	1157	1793	2337	2338	2872	3007	2924	1295	392	1	21	2	4	4	6	9	14	19
Fe^{2+}	mg/L	623	n.m.	826	604	n.m.	1648	1881	n.m.	1779	1456	n.m.	791	245	n.m.	n.m.	n.m.	n.m.	n.m.	n.m.	n.m.	n.m.	n.m.
Fe^{3+}	mg/L	400	n.m.	528	610	n.m.	145	456	n.m.	1093	1551	n.m.	504	147	n.m.	n.m.	n.m.	n.m.	n.m.	n.m.	n.m.	n.m.	n.m.
Co	mg/L	3,07	3,14	3,99	3,43	3,35	4,97	6,31	6,36	7,82	8,17	7,99	3,58	1,09	0,05	0,12	0,03	0,04	0,04	0,05	0,07	0,09	0,11
Ni	mg/L	1,06	1,10	1,39	1,16	1,15	1,71	2,16	2,19	2,70	2,88	2,81	1,23	0,39	0,02	0,05	0,02	0,02	0,02	0,02	0,03	0,04	0,04
Zn	mg/L	122,7	122,7	158,1	138,2	132,7	202,7	265,7	268,9	333,8	354,0	344,4	153,2	43,9	0,5	4,8	1,0	1,3	1,3	1,8	2,5	3,5	4,3
V	µg/L	220	225	290	270	255	388	512	519	629	649	629	272	87	0,33	0,10	0,06	0,05	0,07	0,05	0,04	0,04	0,05
Cr	µg/L	184	181	247	217	207	314	411	408	505	538	531	229	66	1,36	5,54	0,39	0,80	0,98	1,33	2,34	3,70	5,05
Cd	µg/L	264	254	328	280	272	422	543	551	682	734	719	315	88	0,66	10,77	2,63	3,20	2,97	4,21	5,65	7,75	9,49

Table 1: Physical parameters (*measured in situ*), elemental concentrations and Cu isotopic composition for the upstream and downstream sampling points of the Meca River and for the Meca tributary. All concentrations and isotopic were measured in the dissolved fraction (i.e., <0.22 µm). n.m. indicates not measured.

Sampling date	11-May-2015	11-May-2015	12-May-2016	12-May-2016	12-May-2016
Sampling name	MES ME-A 4:00 PM	MES ME-A 10:00 PM	MES ME-A 4:00 AM	MES ME-A 4:00 PM	bed sediment ME-A
unit:	*µg/g*	*µg/g*	*µg/g*	*µg/g*	*µg/g*
δ^{65}Cu (‰)	-0,41 (± 0.03)	-	-	-	-1,92 (± 0.04)
Na	2507	2082	822	3575	10461
Mg	3434	4788	4071	3364	5144
Al	79220	68049	30526	102033	69998
K	18927	16826	4708	25216	19269
Ti	3037	3834	1160	3391	5024
V	115	102	46,7	146	126
Cr	86,1	82,7	43,0	96,5	85,6
Mn	278	439	478	214	275
Fe	112293	132229	66202	101090	129246
Co	38,2	55,2	50,4	20,7	15,6
Ni	27,3	25,8	22,5	28,7	34,9
Cu	669	909	788	479	392
Zn	1126	1554	1928	447	349
As	2831	2689	1653	1984	1009
Se	89	80	75	36	47
Rb	111	103	40	164	73
Sr	78,7	86,3	32,6	96,5	50,1
Y	12,5	15,9	6,8	15,5	19,3
Mo	7,68	8,73	4,15	4,73	3,96
Cd	2,23	3,45	4,00	0,80	0,36
Sn	235	91	185	46	54
Sb	1100	983	776	379	220
Cs	6,72	5,08	2,46	9,03	3,14
Ba	457	473	166	547	288
La	29,6	42,5	12,5	41,7	16,4
Ce	61,2	75,6	24,3	79,7	33,9
Pr	6,94	8,42	2,99	8,86	4,37
Nd	25,3	31,1	10,7	32,8	16,5
Sm	4,79	5,46	2,06	6,12	3,59
Eu	1,13	1,12	0,44	1,13	0,63
Tb	0,47	0,55	0,25	0,55	0,56
Gd	5,61	3,97	2,69	4,25	4,35
Dy	2,51	3,03	1,31	3,02	3,71
Ho	0,50	0,60	0,26	0,60	0,89
ER	1,63	1,97	0,85	1,97	2,71
Tm	0,25	0,31	0,14	0,31	0,43
Yb	1,92	2,25	0,90	2,22	3,03
Lu	0,31	0,36	0,13	0,36	0,45
Pb	7530	9466	4258	4320	1773
Th	10,0	14,9	3,9	16,0	12,1
U	3,45	3,95	1,75	3,13	4,15

Table 2: Elemental concentrations and Cu isotopic composition for the suspended and bed sediments from the Meca River.

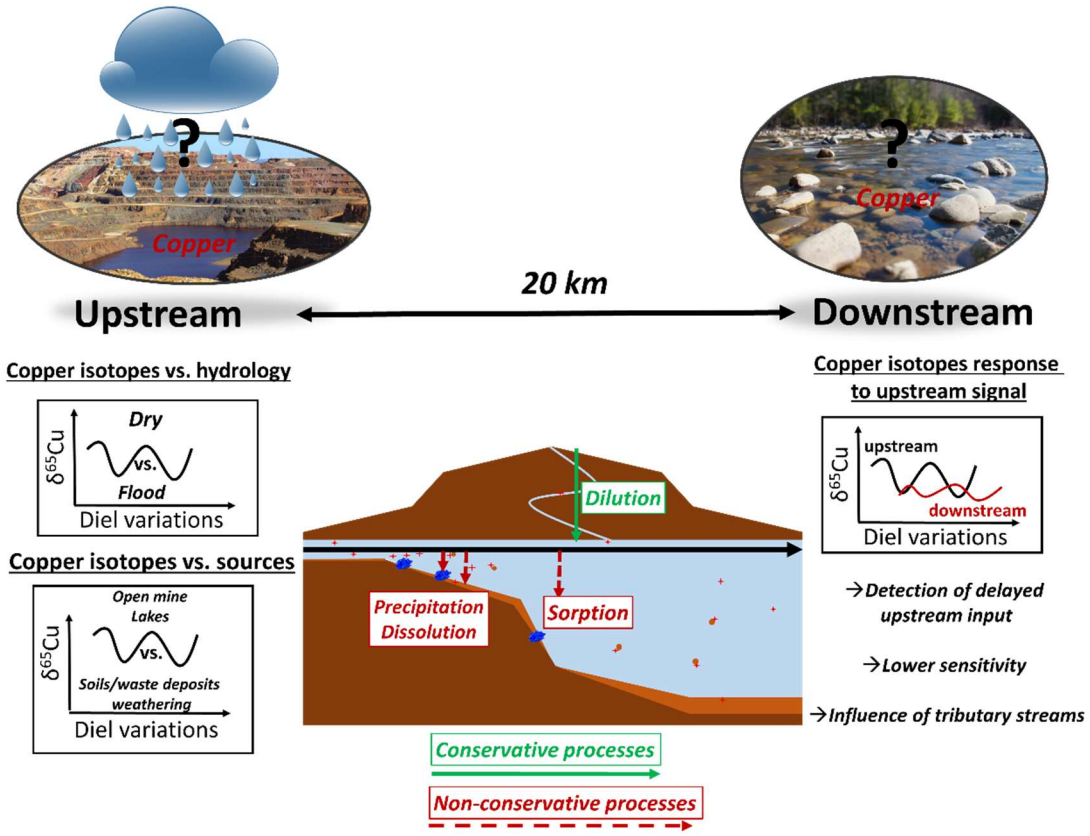
Copper
Copper
20 km
Upstream
Downstream
Copper isotopes vs. hydrology
Dry
vs.
Flood
Diel variations
Copper isotopes vs. sources
Open mine
Lakes
vs.
Soils/waste deposits
weathering
Diel variations
Dilution
Precipitation
Dissolution
Sorption
Copper isotopes response
to upstream signal
upstream
downstream
Diel variations
→Detection of delayed
upstream input
→Lower sensitivity
→Influence of tributary streams
Conservative processes
Non-conservative processes